Alexandria Engineering Journal (2016) xxx, xxx–xxx

HOSTED BY

Alexandria University

Alexandria Engineering Journal

www.elsevier.com/locate/aej
www.sciencedirect.com

ORIGINAL ARTICLE

CFD analysis of flow fields for shrouded wind turbine's diffuser model with different flange angles

Aly M. El-Zahaby, A.E. Kabeel *, S.S. Elsayed, M.F. Obiaa

Mechanical Power Engineering Department, Faculty of Engineering, Tanta University, Egypt

Received 12 June 2016; revised 12 August 2016; accepted 25 August 2016

KEYWORDS

Wind energy;
Small wind turbine;
Flanged diffuser shroud;
CFD

Abstract The present study shows a development and analysis of 2-D axisymmetric CFD model of flanged diffuser that was used as a casing for developed small wind turbines to increase the generated power. The 2-D CFD diffuser model grids are developed by GAMBIT, while the flow field analysis has been carried out using commercial software FLUENT. This study focuses on the effect of flange's angles as a varied parameter on velocity at diffuser entrance. All models have the same dimensions in diffuser length, entrance diameter, exit diameter and flange height but differ in flange angle. Flange angles of these tested models vary from −25° to +25°, where flange angles were measured to vertical axis.

Present model verification indicates a good agreement between present numerical work and previous published experimental work. The numerical simulation shows the created vortices behind flange that cause pressure drop which increases mass flow rate through the diffuser. The results indicate also that the right flange angle at 15° is the optimum angle that accelerates flow at diffuser entrance. The increase of velocity at this optimum flange angles is higher than the case of normal angle, where the expected increase in the generated power by wind turbine can reach 5% more compared with normal flange.

1. Introduction

Combustion of huge quantities of fossil fuels worldwide for power production causes a numerous environmental problems such as acid rain, smog, and climate change due to fossil fuel combustion's emissions.

In recent years, there are global efforts to reduce the worldwide dependence on fossil fuels. So the global awareness has led to a reawakening of interest in renewable energy technology as cleaner power generation methods.

The wind energy is one of the most potential sources of renewable energy. So, there is an increase of manufacturing rate of wind generator turbines with different sizes. One of the differences between large and small scale wind turbines is that small scale wind turbines are generally located where the power is required, often within a built environment, rather than where the wind is most favorable. To yield a reasonable power output from a small scale, the turbines have to improve

* Corresponding author. Tel.: +20 1001543587; fax: +20 403453860.
E-mail addresses: kabeel6@hotmail.com, kabeel6@f-eng.tanta.edu.eg (A.E. Kabeel).

Peer review under responsibility of Faculty of Engineering, Alexandria University.

http://dx.doi.org/10.1016/j.aej.2016.08.036

Nomenclature

A	swept area (m^2)	L	length of diffuser (m)
D_1	diameter of diffuser's inlet (m)	U_ω	free stream wind speed (m/s)
D_2	diameter of diffuser's inlet (m)	U	mean wind speed through diffuser (m/s)
H	height of diffuser's flange (m)	θ	flange's angle (°)

their energy capture, particularly at low wind speeds and be responsive to changes in wind direction.

2. Literature review

It is known that generated power by wind turbines is proportional to the cubic power of the incident wind speed; any small increase in the incident wind causes a large increase in the energy output. Therefore, researchers try to increase wind speed locally at wind turbine blades by different techniques. Shrouded or ducted wind turbine is one of important used techniques to improve power captured.

Lilley and Railbird [1] performed a theoretical study to obtain the gain of generated power output from a fully ducted land type wind turbine that was 65 % of the maximum power output of the ideal bare wind turbine. Igrae [2] used a blowing at shroud intake and airfoil shaped ring-flap at exit of diffuser as two techniques to prevent flow separation and increase power generation. The blowing increased the output power by 20%, while using airfoil shaped ring-flap produced an increase in power by 65%. Igrae [3] also did experimental studies on a shrouded aero generator in wind tunnel. The power generated from his model was about twice the output power generated from an ideal wind turbine working under the same conditions. Foreman et al. [4] investigate a technical and economic study about diffuser augmented wind turbine "DAWT". The study obtained significant power augmentation from DAWT approaching twice of power generated by bare wind turbine. The increase of power was produced due to low pressure at diffuser exit that pumps much larger amounts of air through a DAWT than a conventional wind turbine. Gilbert et al. [5] study the parameters that affect on the performance of the diffuser system and examined it in wind tunnel. Their first generation of DAWT provided about twice the power of a conventional wind energy conversion system "WECS" with the same turbine diameter and wind velocity and Maximum augmentation ratio reaches 3. Igrae [6] discusses the design and performance of an axial flow turbine which is the most suitable for the proposed shrouds. His turbine produced a fairly stable output for varying wind speeds while exhibiting a fairly high efficiency. The augmentation factor of power generation was in the range of 2–4. Phillips et al. [7] investigate theoretical, numerical and experimental tests on Vortec 7 wind turbine and compared it with previous experimental work. It was obtained that the CFD agreed quite well with field measurements. Many of the field results also agreed with the previous experimental result. Hansen et al. [8] compared the CFD computations of a bare turbine with the theoretical expression for the power coefficient as a function of the thrust coefficient. The actuator disk approach is sufficient for modeling the rotor of wind turbine and also was seen that the Betz limit can be exceeded with a ratio corresponding to the relative increase in mass flow rate through the rotor when using diffuser for rotor. Abe and Ohya [9] study the flow fields around flanged diffuser using CFD to develop small-type wind turbines under 1.5 kW. Comparison of the computed results with the corresponding experimental data shows that their calculation had the capability of providing reasonable predictions for the complex turbulent flows. It was shown that the performance of a flanged diffuser strongly depends on the loading coefficient as well as the opening angle. Abe et al. [10] carried out experimental and numerical investigations for flow fields of a small wind turbine with a flanged diffuser. The results show that the power coefficient of the diffuser shrouded wind turbine was about four times as high as that of the bare wind turbine, and the power augmentation of this kind of wind turbine was mainly caused by the acceleration of the approaching wind by a flanged diffuser. Matsushima et al. [11] studied experimentally and numerically the effects of a frustum-shaped diffuser on the output power of small wind turbine. Their results showed that the used diffuser parameters were able to increase the maximum wind speed at diffuser entrance by around 1.7 times and maximum energy production ratio of around 2.4 times was obtained by collecting wind energy in the turbine. Ohya et al. [12] found hollow-structure diffuser is as effective as the shroud form wind turbine for collecting and accelerating the wind. Also they found when using a flange of proper height attached to the outer periphery of the diffuser exit, a remarkable increase in wind speed of 1.6–2.4 times that of the approaching wind speed power augmentation for a given turbine diameter and wind speed by a factor of about 4–5 compared to a bare wind turbine due to a low-pressure region in the exit area of the diffuser by vortex formation and draws the wind into the diffuser. Wang et al. [13] used a scoop to improve energy capture from wind turbine at low wind speed. Their study used physical tests conducted in a boundary layer wind tunnel and commercial CFD code to get an optimal design of a scoop. The final design of scoop boosted the airflow speed by a factor of 1.5 times equivalent to an increase in power output of 2.2 times with the same swept area. Raj and Nair [14] did a development and analysis on a 3D CFD model of a shrouded wind turbine with flange by GAMBIT and analysis had been carried out in commercial software FLUENT. Their result showed a good agreement between their numerical study and previous experimental work. Ohya and Karasudani [15] developed a very compact brimmed diffuser that achieved two to threefold increase in output power compared to conventional wind turbines. Kardous et al. [16] investigate a numerical simulation and PIV simulation to get a better understanding of the effect of the flange height on wind velocity increase at the inlet section of an empty flanged diffuser. It is shown that the flange contributed with diffuser to increase wind at its inlet section. The wind

Please cite this article in press as: A.M. El-Zahaby et al., CFD analysis of flow fields for shrouded wind turbine's diffuser model with different flange angles, Alexandria Eng. J. (2016), http://dx.doi.org/10.1016/j.aej.2016.08.036

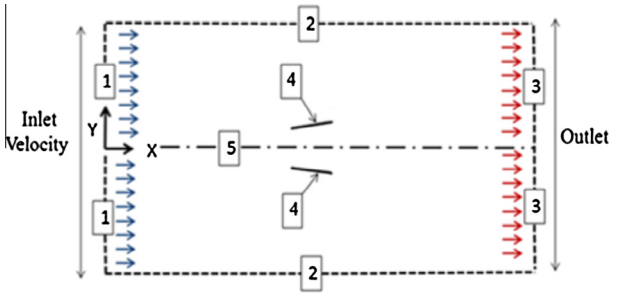

Figure 1 Schematic diagram for the problem.

Table 1 Results from grid dependency simulations.

No.	Total number of grid points	U_c (at $x/D_i = 5$ With $U_i/U_O = 20/10$)	Diff. %
1	11,392	19.15977 m/s	–
2	14,700	18.92985 m/s	1.2
3	19,440	18.924175 m/s	0.03
4	27,900	18.9241 m/s	0.0004

velocity increase rate by diffuser without flange was about 58% while for the flanged one, this rate ranged from 64% to 81% and the flange height seemed to be without significant effect to increase wind velocity beyond $H_c/D_a = 0.1$ (H_c is flange height and D_a throat diameter).

In the present study a numerical simulation by commercial CFD package describes the effect of diffuser flange angles on flow speed at diffuser entrance and getting an optimum angle that occur at its maximum speed . Also the numerical study shows flow field around diffuser at different cases.

3. Numerical work

In present work, commercial package "FLUENT 6.3" is used to transform and solve the partial differential equations based on the "SIMPLE" algorithm introduced by Patanker [17].

3.1. Governing equations

The governing equations that describe the present problem configuration are continuity, momentum, and energy; the turbulence model used in this study is (K-ε model) expressed by the full elliptic Navier–Stokes partial differential equations which are available in text books. For the present problem, the flow is assumed to be steady, turbulent, incompressible and two-dimensional whereas air is taken as a working medium. For standard K-ε model, a common method employs the Boussinesq hypothesis to relate the Reynolds stresses to the mean velocity gradient.

$$-\overline{\rho u_i' u_j'} = \mu_t\left[\frac{\partial u_i}{\partial X_j}+\frac{\partial u_j}{\partial u_i}\right]-\frac{2}{3}\left[\rho K+\frac{\partial u_i}{\partial X_i}\right]\delta_{ij} \tag{1}$$

where δ_{ij} is the Kronecker delta function $\delta_{ij} = 1$ for $i = j$, otherwise $\delta_{ij} = 0$.

μ is the dynamic viscosity of the fluid, and $u_i' u_j'$ is the turbulent Reynolds stress.

After modeling the Reynolds stresses term the above governing equations can be simplified as follows:

Continuity Equation

$$\frac{\partial(\rho u)}{\partial x}+\frac{\partial(\rho v)}{\partial y}=0.0 \tag{2}$$

Momentum Equations

x – Direction

$$\frac{\partial(\rho u^2)}{\partial x}+\frac{\partial(\rho uv)}{\partial y}=-\frac{\partial P}{\partial x}+\frac{\partial}{\partial x}\left[\mu_e\frac{\partial u}{\partial x}\right]+\frac{\partial}{\partial y}\left[\mu_e\frac{\partial u}{\partial y}\right]-\frac{2}{3}\frac{\partial}{\partial x}(\rho K)+\rho g_x \tag{3}$$

y – Direction

$$\frac{\partial(\rho uv)}{\partial x}+\frac{\partial(\rho v^2)}{\partial y}=-\frac{\partial P}{\partial y}+\frac{\partial}{\partial x}\left[\mu_e\frac{\partial v}{\partial x}\right]+\frac{\partial}{\partial y}\left[\mu_e\frac{\partial v}{\partial y}\right]-\frac{2}{3}\frac{\partial}{\partial y}(\rho K) \tag{4}$$

Energy Equation

$$\frac{\partial(\rho uT)}{\partial x}+\frac{\partial(\rho vT)}{\partial y}=\frac{\partial}{\partial x}\left[\Gamma_e\frac{\partial T}{\partial x}\right]+\frac{\partial}{\partial y}\left[\Gamma_e\frac{\partial T}{\partial y}\right]+S_T \tag{5}$$

where

μ_e is the effective viscosity, $\mu_e = \mu + \mu_t$

μ_t is the turbulent viscosity which is calculated from the following relation: $\mu_t = \rho C_\mu \frac{K^2}{\varepsilon}$

Turbulence Equations

K – Equation

$$\frac{\partial(\rho uK)}{\partial x}+\frac{\partial(\rho vK)}{\partial y}=\frac{\partial}{\partial x}\left[\left(\mu+\frac{\mu_t}{\sigma_K}\right)\frac{\partial K}{\partial x}\right]+\frac{\partial}{\partial y}\left[\left(\mu+\frac{\mu_t}{\sigma_K}\right)\frac{\partial K}{\partial y}\right]-g\frac{\mu_t}{Pr_t}\frac{\partial \rho}{\partial x}+\mu_t\left\{2\left[\left(\frac{\partial u}{\partial x}\right)^2+\left(\frac{\partial v}{\partial y}\right)^2\right]+\left(\frac{\partial u}{\partial y}+\frac{\partial v}{\partial x}\right)^2\right\}-\rho\varepsilon \tag{6}$$

ε-Equation

$$\frac{\partial(\rho u\varepsilon)}{\partial x}+\frac{\partial(\rho v\varepsilon)}{\partial y}=\frac{\partial}{\partial x}\left[\left(\mu+\frac{\mu_t}{\sigma_\varepsilon}\right)\frac{\partial \varepsilon}{\partial x}\right]+\frac{\partial}{\partial y}\left[\left(\mu+\frac{\mu_t}{\sigma_\varepsilon}\right)\frac{\partial \varepsilon}{\partial y}\right]-C_{1\varepsilon}g\frac{\varepsilon}{K}\frac{\mu_t}{Pr_t}\frac{\partial \rho}{\partial x}+C_{1\varepsilon}\frac{\varepsilon}{K}\mu_t\left\{2\left[\left(\frac{\partial u}{\partial x}\right)^2+\left(\frac{\partial v}{\partial y}\right)^2\right]+\left(\frac{\partial u}{\partial y}+\frac{\partial v}{\partial x}\right)^2\right\}-C_{2\varepsilon}\rho\frac{\varepsilon^2}{K} \tag{7}$$

3.2. Boundary conditions

Due to symmetrical nature of the configuration as shown in Fig. 1, the flow is considered to be two-dimensional flow

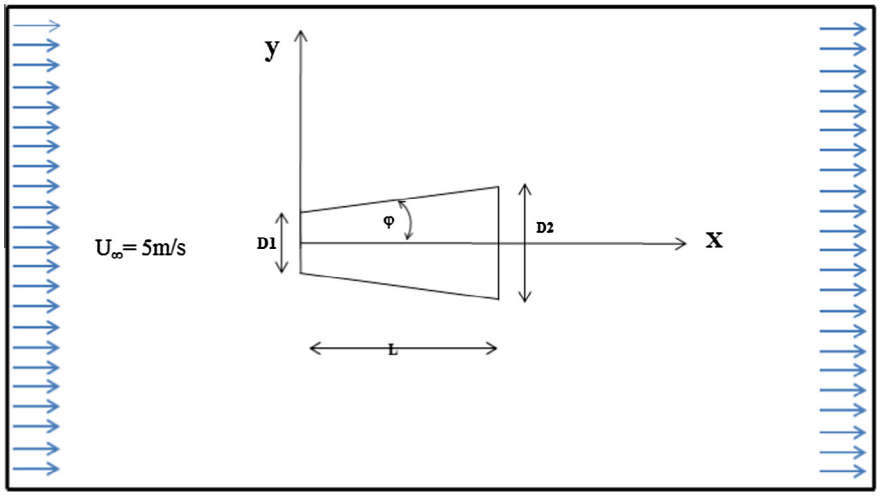

Figure 2 Schematic of diffuser model is hanged in test section of open wind tunnel.

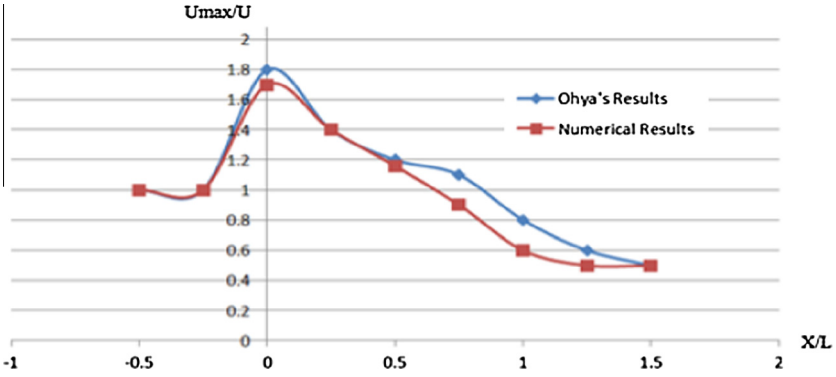

Figure 3 Fluent's numerical result and Ohya's experimental results' [1] curves.

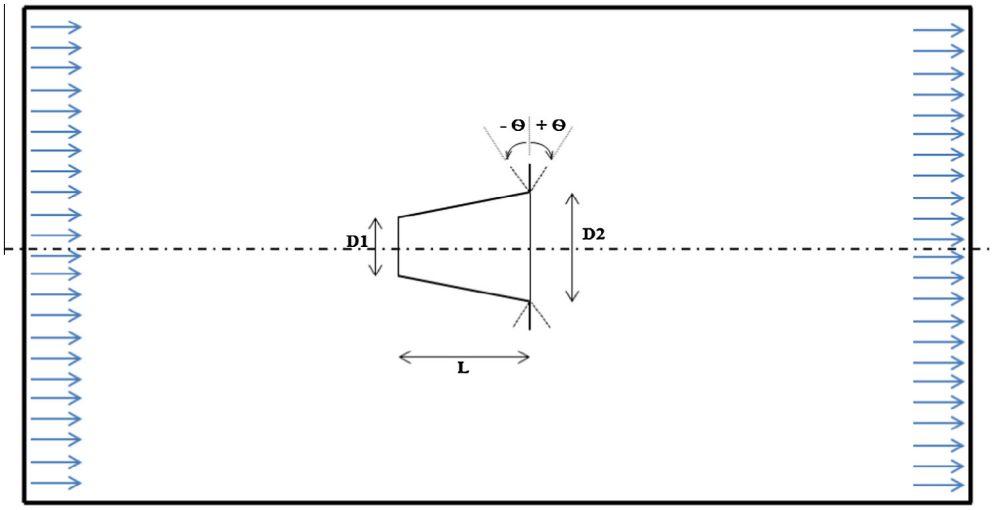

Figure 4 Schematic of diffuser models hanged at center of test section.

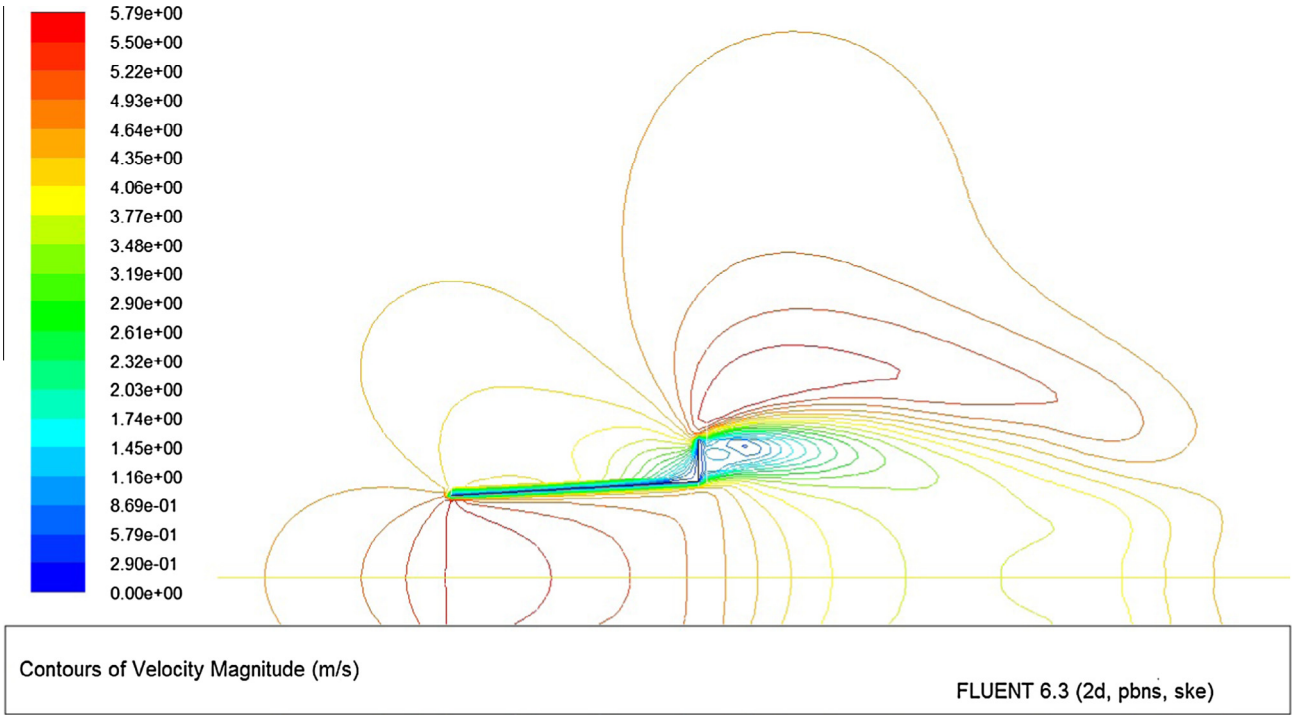

Figure 5 Velocity magnitude contour of flow field at flange angle $\theta = 0°$.

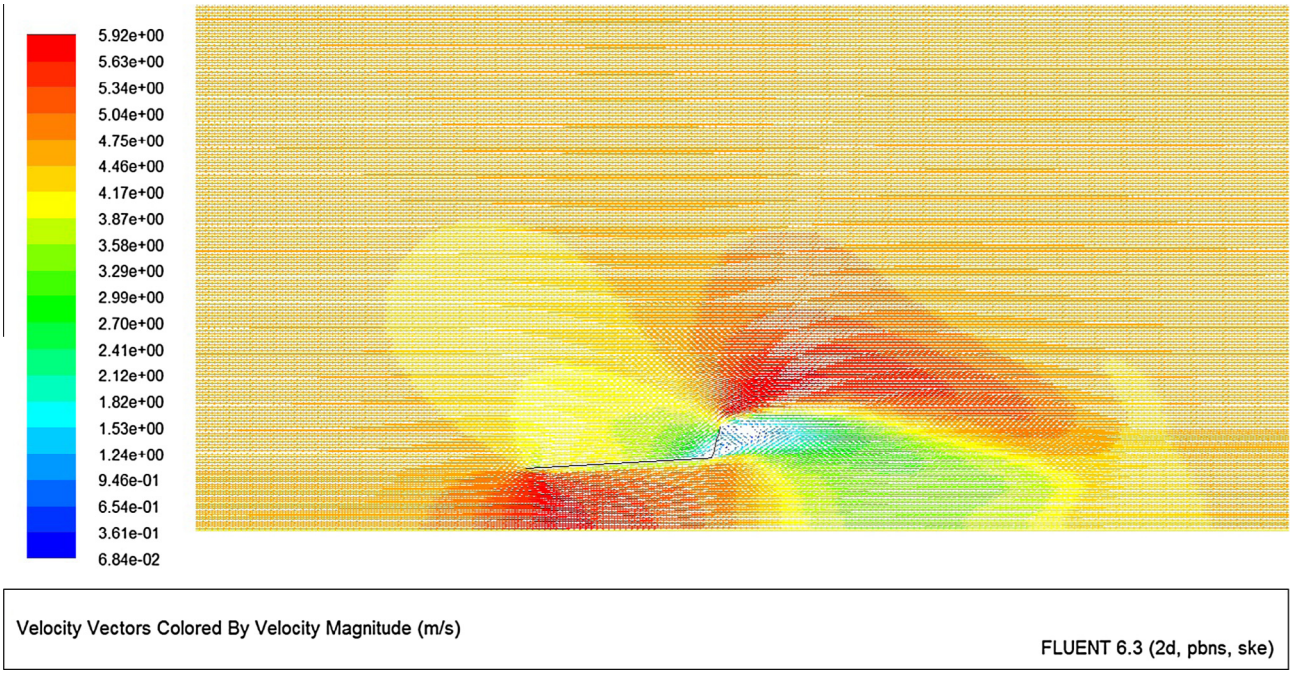

Figure 6 Velocity vector contour of flow field at flange angle $\theta = +15°$.

(2D) in the x-y plane, with no changes of problem variables in the z-direction.

Boundary conditions are a very important step in the numerical solution. It depends on some assumptions, so, it should be taken when putting boundary conditions. Fig. 1 shows the problem boundary condition.

For the boundary (1), inlet-velocity, $u = u_\infty$, $v = 0.0$

For the boundary (2), Wall, no slip boundary condition $u = 0.0$, $v = 0.0$

For the boundary (3). Outlet flow, in compressible flow, flow in = flow out

For the boundary (4), Wall(Body), no slip boundary condition $u = 0.0$, $v = 0.0$

For the boundary (5), Symmetric axis.

Please cite this article in press as: A.M. El-Zahaby et al., CFD analysis of flow fields for shrouded wind turbine's diffuser model with different flange angles, Alexandria Eng. J. (2016), http://dx.doi.org/10.1016/j.aej.2016.08.036

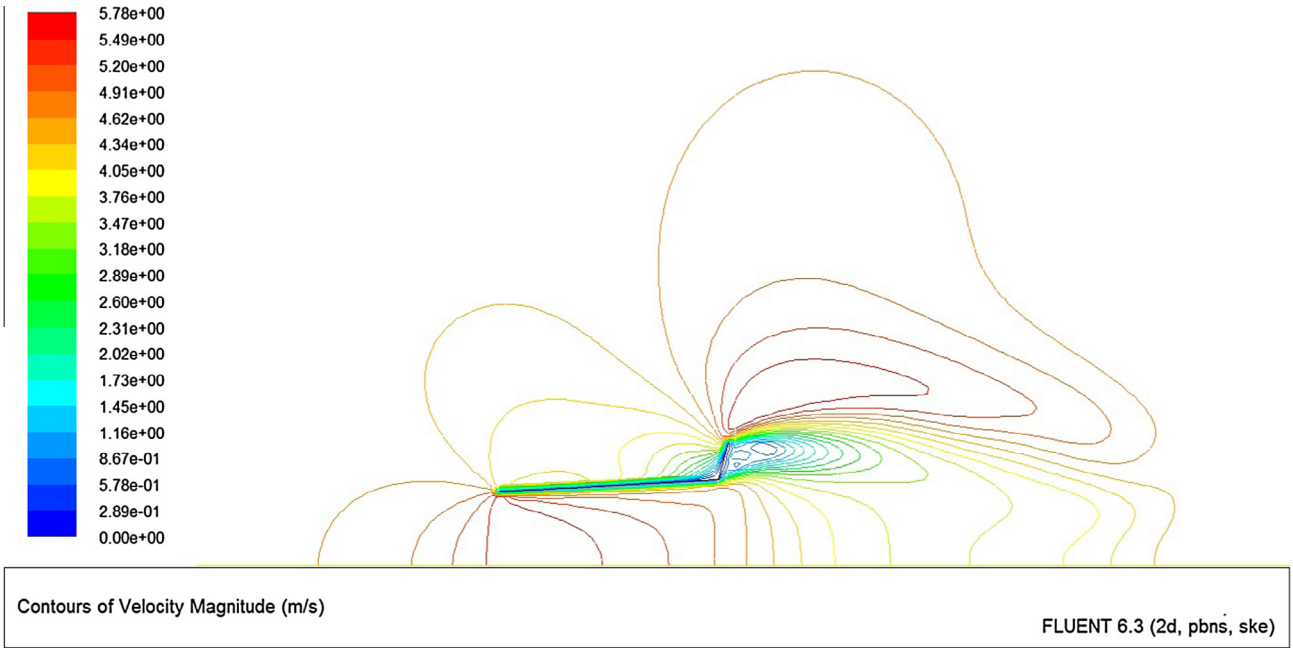

Figure 7 Velocity magnitude contour of flow field at flange angle $\theta = +15°$.

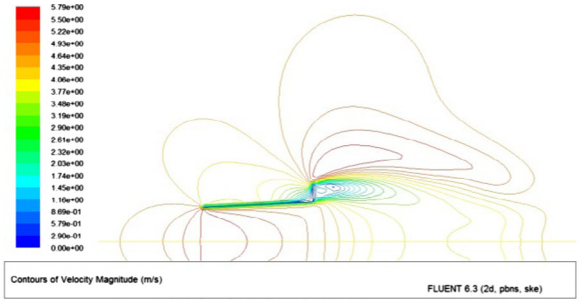

a. Flange angle at $\Theta = 0°$

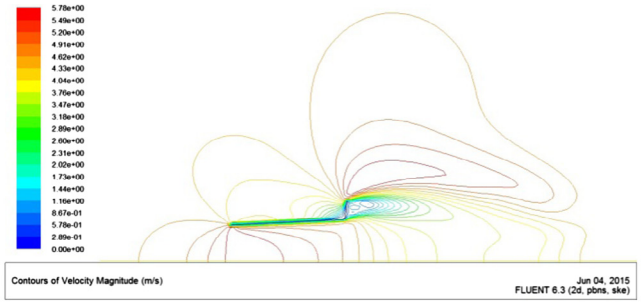

b. Flange angle at $\Theta = 5°$

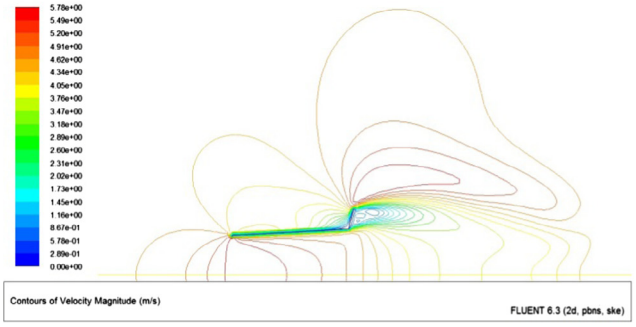

c- Flange angle at $\Theta = 15°$

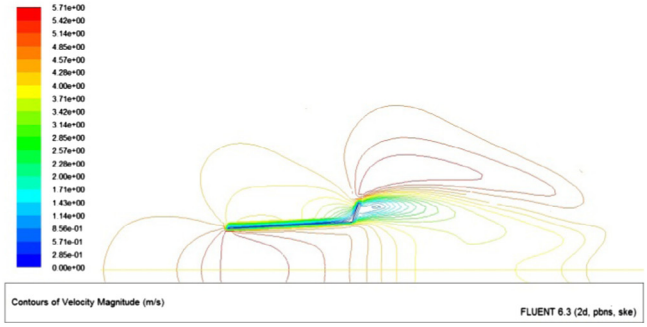

d- Flange angle at $\Theta = 25°$

Figure 8 Velocity magnitude contours for right angles compared with $\theta = 0°$.

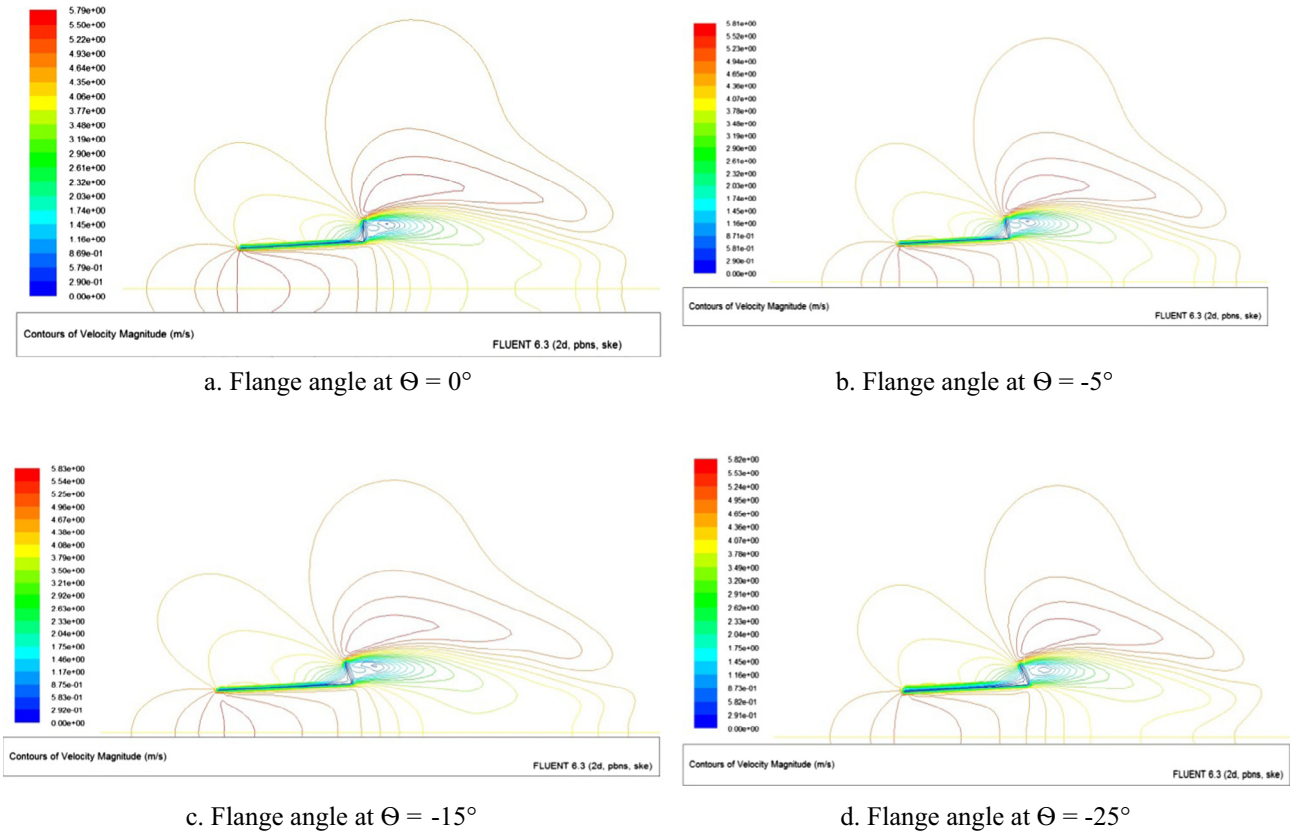

a. Flange angle at Θ = 0°

b. Flange angle at Θ = -5°

c. Flange angle at Θ = -15°

d. Flange angle at Θ = -25°

Figure 9 Velocity magnitude contours for left angles compared with $\theta = 0°$.

3.3. Mesh test

The problem domain discretization is achieved by dividing the domain boundaries into a finite number of nodes and applying a mesh generation code to create a finite number of cells. The cells number and size are depending on the number of the nodes in domain boundaries and mesh type, structured or unstructured. In the problem under investigation, the domain is divided into quadrilateral cells; the streamwise direction is divided into 225 cells while the radial direction is divided into 124 cells. Number of the nodes in the mesh generated is 27,900 nodes. Table 1, summarizes the results obtained during the grid dependency tests. Based on its tests, it is found that, the grid size (Δx and Δy) network of 2 mm * 2 mm will be used in all the computations.

3.4. Model verification

This model is verified with experimental results that were done by Ohya et al. [12]. A subsonic open wind tunnel is used to avoid the blockage effect with test section: 3.6 m wide, 2 m high and 15 m long with the maximum wind velocity of 30 m/s. Hot wire I-type used to measure velocity distributions of wind velocity, U. The smoke-wire technique was employed for the flow visualization experiment.

The inner flow of diffuser model with both ends of the hollow structure model is examined, the narrow end is a square cross-section of $D_1 = 12$ cm and the wide end is $D_2 = 24$ cm. The area ratio μ is defined as the outlet area/inlet area = 4, and the angle of inclination φ is 3.71. The length ratio $L/D = 7.7$, here, L is the model length shown in Fig. 2.

It is obtained from experimental result a remarkable effect on the collection and acceleration of the approaching wind. A maximum of $U/U_\infty = 1.8$ is shown in the neighborhood immediately after the entrance. By Gambit, the diffuser model is prepared with same dimension under same condition to be simulated by Fluent. Fluent options help us to find velocity magnitude at any points of domain, so it is easy to compare numerical result with experimental one. Two curves at Fig. 3 show velocity ratio between maximum local velocity and free stream velocity $U = 5$ m/s across diffuser length. The difference between the two curves that is shown in Fig. 3 varies from 0.12% to 8.3%. These values indicate a good agreement between present numerical study by fluent package and Ohya's experimental results.

4. Numerical study

In this part, the effects of diffuser flange's angles are simulated by Fluent package. The objective of this study was determining an optimum flange's angle that causes maximum increase of inlet's velocity and consequently more generated power. Diffuser models that are tested have same geometry but with different flange angles. The following dimensions are fixed dimensions for all models: diffuser's length $L = 9$ cm, inlet diameter $D_1 = 6$ cm, exit diameter $D_2 = 7$ cm and Flange height $h = 1.5$ cm. The flange's angles vary from −25 to +25 with step 5° as shown in Fig. 4.

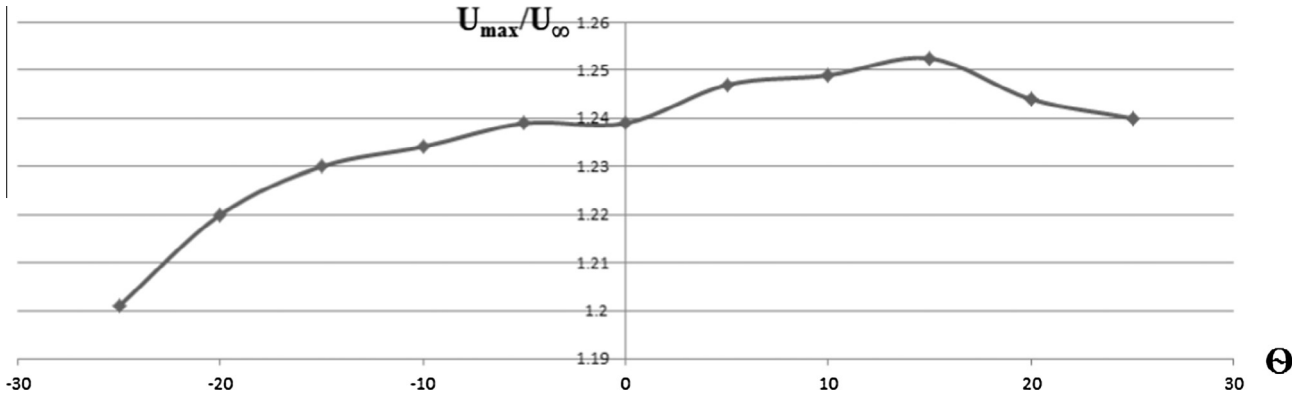

Figure 10 Curve obtained relation of velocity increase at diffuser entrance and flange angles.

5. Numerical results

The CFD FLUENT Modeling provides detailed information and visual indication of air flows. These results help to validate the phenomenon of velocity increase when using flange at diffuser exit and also to have the optimum flange angle which causes the maximum increase of velocity at diffuser entrance. FlUENT's results include velocity magnitude at any point in the physical domain. Also it is easy to extract velocity vectors and static pressure contours as shown in the following figures. Fig. 5 shows the velocity vectors contour inside and around the diffuser with flange angle $\theta = 0°$ and at free stream velocity $U_\infty = 4.5$ m/s, while Fig. 5 shows the velocity magnitude contour in the same domain for the same conditions.

Fig. 6 shows the velocity vectors, velocity magnitude at the same free stream velocity = 4.5 m/s but with flange diffuser angle $\theta = +15°$.

The previous figures indicate an increase of velocity at diffuser entrance and decrease of velocity with negative pressure area behind flange, Fig. 7. As example for $\theta = +15°$ the velocity reaches a value of 5.63 m/s at diffuser entrance, Fig. 7. The negative pressure area is generated by vortices due to flange effect and diffuser shape. Also it is noticed that the velocity increase at $\theta = +15°$ is larger than velocity increase at normal case $\theta = 0°$. The main reason for this velocity increase is a pressure difference between diffuser entrance and diffuser exit.

While Fig. 8 shows the velocity magnitude contour for positive flange angles compared with zero angles, Fig. 9 shows the velocity magnitude contour for negative flange angles compared with zero angles.

Using the numerical results extracted from Figs. 8 and 9, it is possible to draw the dimensionless air velocity variation at diffuser entrance related free stream velocity, Fig. 10. It is concluded from Fig. 10 that the optimum flange angle θ is obtained at $+15°$, at which there is the maximum entrance velocity increase.

6. Conclusions

The present numerical study using FLUENT package shows the flow characteristics inside diffuser model and around it for different flange angles, where the flowing conclusions are obtained:

(1) There is a good agreement between numerical results by FLUENT package and published experimental results.
(2) The present numerical results validate the presence of vortices behind diffuser flange that causes negative pressure region, and consequently diffuser entrance air velocity increase.
(3) Present study indicates an optimum flange angle $\theta = +15°$, where maximum entrance air velocity increase is reached.
(4) The expected power increase ratio at optimum flange angle reaches a value of 1.953 related to the expected power of bare turbine, while the expected power increase ratio at normal flange reaches 1.903, that means the enhancement in power generation is about 5% due to optimum flange angle.

References

[1] G.M. Lilley, W.J. Rainbird, A preliminary report on the design and performance of ducted windmills, Report 102, April 1956, College of Aeronautics, Cranfield, England. (Also available as Technical Report CIT ll9, 1957, Electrical Research Assoc., Leatherhead, England).
[2] Ozer Igra, Compact shrouds for wind turbines, Energy Convers. 16 (4) (1977) 149–157.
[3] Ozer Igra, The shrouded aerogenerator, Energy 2 (4) (1977) 429–439.
[4] Foreman, B. Gilbert, R.A. Oman, Diffuser augmentation of wind turbines, Sol. Energy 20 (1978).
[5] B.l. Gilbert et al, Fluid dynamics of diffuser-augmented wind turbines, J. Energy 2 (6) (1978) 368–374.
[6] Ozer Igra, Research and development for shrouded wind turbines, Energy Convers. Manage. 21 (1981) 13–48.
[7] D.G. Phillips, P.J. Richards, G.D. Mallinson, R.G.J. Flay, Aerodynamic analysis and monitoring of the Vortec 7 diffuser-augmented wind turbine, in: IPENZ Conference, 1998.
[8] M.O.L. Hansen, N.N. Sorensen, R.G.J. Flay, Effect of placing a diffuser around a wind turbine, J. Fluid Mech. 3 (2000) 207–213.
[9] K. Abe, Y. Ohya, An investigation of flow fields around flanged diffusers using CFD, J. Wind Eng. Ind. Aerodyn. 92 (2004) 315–330.
[10] K. Abe, M. Nishida, M.A. Sakurai, Y. Ohya, H. Kihara, E. Wada, K. Sato, Experimental and numerical investigations of flow fields behind a small-type wind turbine with flanged diffuser, J. Wind Eng. Ind. Aerodyn. 93 (2005) 951–970.

Please cite this article in press as: A.M. El-Zahaby et al., CFD analysis of flow fields for shrouded wind turbine's diffuser model with different flange angles, Alexandria Eng. J. (2016), http://dx.doi.org/10.1016/j.aej.2016.08.036

[11] Toshio Matsushima, Shinya Takagi, Seiichi Muroyama, Characteristics of a highly efficient propeller type small wind turbine with a diffuser, Renewable Energy 31 (2006) 1343–1354.
[12] Yuji Ohyaa, Takashi Karasudani, Akira Sakurai, Masahiro Inoue Ken-ichiAbb, Development of a shrouded wind turbine with a flanged diffuser, J. Wind Eng. Ind. Aerodyn. 96 (2008) (2008) 524–539.
[13] F. Wang, L. Bai, J. Fletcher, J. Whiteford, D. Cullen, The methodology for aerodynamic study on a small domestic wind turbine with scoop, J. Wind Eng. Ind. Aerodyn. 96 (2008) 1–24.
[14] Ullas Innocent Raj, Anitha S. Nair, development of 3d CFD model of a shrouded wind turbine, in: 10th National Conference on Technological Trends (NCTT09) 6–7 Nov 2009.
[15] Yuji Ohya, Takashi Karasudani, A shrouded wind turbine generating high output power with wind-lens technology, Energies 3 (2010) 634–649.
[16] M. Kardous, R. Chaker, F. Aloui, S. Ben Nasrallah, On the dependence of an empty flanged diffuser performance on flange height: Numerical simulations and PIV visualizations, Renewable Energy 56 (2013) 123e128.
[17] FLUENT 6.3 User's Guide.

Please cite this article in press as: A.M. El-Zahaby et al., CFD analysis of flow fields for shrouded wind turbine's diffuser model with different flange angles, Alexandria Eng. J. (2016), http://dx.doi.org/10.1016/j.aej.2016.08.036